Supplementary materials

Structure-guided stereoselectivity inversion of a short-chain dehydrogenase/reductase towards halogenated acetophenones

Authors and Affiliation:

Aipeng Li[1], Lidan Ye[1,2], Xiaohong Yang[1], Chengcheng Yang[1], Jiali Gu[3], Hongwei Yu[1]*

[1]*Institute of Bioengineering, College of Chemical and Biological Engineering, Zhejiang University, Hangzhou 310027, PR China*

[2]*Key Laboratory of Biomass Chemical Engineering of Ministry of Education, Zhejiang University, Hangzhou 310027, PR China*

[3]*College of Life Science, Department of Materials Chemistry, Huzhou University, Huzhou 313000, PR China*

*** Corresponding author:**

Institute of Bioengineering, College of Chemical and Biological Engineering, Zhejiang University, Hangzhou 310027, PR China.

Tel.: +86 571 8795 1873; Fax: +86 571 8795 1873.

E-mail: yuhongwei@zju.edu.cn

Table of Content

Materials and methods

Materials

Halogenated acetophenones and their corresponding chiral alcohols of analytical grade were purchased from J&K Scientific Ltd. (Beijing, China) or Sigma-Aldrich (Shanghai, China). NADH disodium salt was purchased from Sangon (Shanghai, China). The enzymes used in molecular operation such as PrimeSTAR^{TM} HS DNA polymerase, Taq DNA polymerase, restriction endonucleases (*BamH*I and *Xho*I) and T4 DNA ligase were purchased from TaKaRa (Dalian, China). Genomic DNA purification kit was obtained from Dongsheng, China. Gel extraction kit and plasmid miniprep kit were obtained from Axygen, China. Primers were synthesized by Invitrogen, China. Ni-NTA column was purchased from GE Healthcare Bio-Science, Sweden. The other chemical reagents used were all of analytical grade and obtained from local companies.

Cloning of recombinant PpYSDR

Genomic DNA was extracted from *Pseudomonas putida* ATCC 12633 using genomic DNA purification kit described above. The gene encoding PpYSDR (GenBank database under accession number BAN52518.1) was amplified by PCR using PrimeSTAR^{TM} HS DNA polymerase with the following primers: PpYSDRF-*BamH*I (5'-GCTGAGGATCCATGGCTAATGCAAAAACCGC-3') and PpYSDRR-*Xho*I (5'-GCATCCTCGAGTCACCAGACCAAGGGTTCGC-3'). The PCR product was double-digested with *BamH*I and *Xho*I, followed by ligation into the expression vector pET30a. The resulting plasmid, harboring the *Ppysdr* gene, was designated pET30a-PpYSDR. The plasmid pET30a-PpYSDR was transformed into *Escherichia coli* BL21(DE3) which was then spread on Luria-Bertani agar plates containing 50 μg/ml kanamycin. The single colony with recombinant plasmid pET30a containing the *Ppysdr* gene was verified by DNA sequencing.

Construction of mutants

The pET30a plasmids containing the recombinant PpYSDR gene were used as the templates for polymerase chain reaction (PCR)-based site-directed mutagenesis using the QuikChange™ method (Stratagene, La Jolla, CA). The PCR primers are listed in Table S1. The PCR mixture contained 15 ng of template plasmid, 5 μL of 5× PrimerSTAR™ Buffer (Mg^{2+} plus), 2 μL of dNTP (2.5 mM each), 1 μL of each primer (10 μM), and 0.5 μL of PrimerSTAR™ HS polymerase (2.5 U/μL) in a total volume of 25 μL. The PCR reaction was carried out under the following conditions: 98 °C denaturation for 1 min, 20 cycles of 98 °C denaturation for 10 s, 55 °C annealing for 10 s, and 72 °C extension for 7 min. The PCR product was purified and then digested with *Dpn* I, which specifically cleaves the adenine methylated template. The digestion mixture contained 17 μL of purified PCR product, 2 μL of 10 × T Buffer and 1 μL of *Dpn* I (10 U/μL). The digestion was conducted at 37 °C for 1 h. Then the mixture was transformed into competent cells (*E.coli* BL21 (DE3)) using the heat shock method at 42 °C for 90 s. Finally, colonies were cultured on Luria-Bertani agar plates. The entire mutant gene was sequenced to verify that no other alterations were introduced into the nucleotide sequence.

Overexpression and purification of enzymes

All mutants were grown at 37°C in Luria-Bertani medium containing 50 μg/ml kanamycin until the optical density at 600 nm reached 0.6-0.8, then gene expression was induced with 0.1 mM isopropyl β-D-1-thiogalactopyranoside (IPTG). The cells were subsequently cultured at 25°C for 5 h and then harvested by centrifugation. The pellet was washed and resuspended in 100 mM Na_2HPO_4-NaH_2PO_4 buffer (pH 8.0) and disrupted by ultrasonication for 10 min. The cell lysate was centrifuged at 12, 000 rpm for 10 min, and the supernatant was applied to a Ni-NTA affinity chromatography column equilibrated with binding buffer (20 mM sodium phosphate, 0.5 M NaCl and 20 mM imidazole, pH 7.4). The bound enzyme was eluted with

elution buffer (20 mM sodium phosphate, 0.5 M NaCl and 0.5 M imidazole, pH 7.4), and then the fractions containing PpYSDR were desalted with 100 mM Na_2HPO_4-NaH_2PO_4 (pH 7.5) by a HisTrap desalting column and stored at 4 °C. SDS-PAGE was used to verify the successful expression and purification of PpYSDR and its variants. Protein concentrations were quantified via the method of Bradford[1] using BSA as the protein standard.

Circular dichroism spectroscopy

Circular dichroism (CD) spectra were obtained using a Jasco J-815 circular dichroism spectrometer (Japan Spectroscopic, Tokyo) at room temperature. CD spectra for the wild-type PpYSDR and variants were recorded in Na_2HPO_4-NaH_2PO_4 buffer (100 mM, pH 7.5) in a quartz cuvette with a 0.1 cm light path over a wavelength range of 190-260 nm. CD spectra were analyzed for percentage of α-helix and β-sheet structure.

Enzyme assay and kinetic analysis

The catalytic activity was assayed spectrophotometrically at 30 °C by monitoring the change in absorbance at 340 nm. One unit of enzyme activity was defined as the amount of enzyme catalyzing the oxidation of 1 μmol of NADH per minute under measurement conditions. The apparent kinetic parameters for the reduction of halogenated acetophenones were calculated by measuring the enzyme activity at different substrate concentrations. The assay mixture (1.0 ml) for the reduction of halogenated acetophenones contained 0.3 mM NADH and 100 μl isopropanol in 100 mM Na2HPO4-NaH2PO4 buffer (pH 7.5). Substrate concentrations used were **1a** (0 to 30 mM), **1b** (0 to 10 mM), **1c** (0 to 0.5 mM), **1d** (0 to 0.2 mM), **1e** (0 to 10 mM), and **1f** (0 to 1.0 mM). The constants were calculated from the Lineweaver-Burk double-reciprocal plot.

Asymmetric reduction of halogenated acetophenones

The standard reaction mixture contained 10 mM halogenated acetophenones, Na_2HPO_4-NaH_2PO_4 buffer (100 mM, pH 7.0), 2.5 mM NADH and an appropriate amount of the enzyme in a total volume of 1.0 ml. The reactions were carried out at 30°C with shaking at 200 rpm. Samples were extracted with ethyl acetate and the organic layer was dried over anhydrous Na_2SO_4. The conversion and enantiomeric excess of product (ee_p) were determined by chiral gas chromatography (GC) analyses. All experiments were conducted in triplicate if not otherwise specified.

Analytical methods

Chiral analysis of halogenated acetophenones and corresponding chiral alcohols was performed on a GC-9790 gas chromatography system (Wenling, China) equipped with an FID detector using nitrogen as the carrier gas. The injector and detector temperatures were both set at 240°C. Prochiral ketones and corresponding chiral alcohols were determined on a Cyclodex-B chiral capillary column (Agilent, USA, 30 m × 0.32 mm, 0.25 μm film thickness) or a Hydrodex β-TBDAc chiral column (Macherey-Nagel, Germany, 25 m × 0.25 mm, 0.25 μm film thickness). The column temperature program and the retention times were the same as in our previous reports[2].

Molecular homology modeling and docking

The three-dimensional homology models of PpYSDR and EbSDR8 were generated using Build Homology Models (MODELER). Structural refinement of the model was performed by energy minimization, and molecular dynamics simulation was conducted as previously described[3]. The structure models of variants were set up using Swiss-PDB Viewer (http://spdbv.vital-it.ch/). The docking experiments of WT and variants towards halogen substituted acetophenones were performed with AutoDock Vina 1.1.2[4]. Docking runs were carried out using the standard parameters of the program for interactive growing and subsequent scoring, except for the parameters for setting grid box dimensions and center. The values of grid box dimensions and centers in docking studies were set based on the known substrate-binding pocket.

Supplementary Tables

Table S1 PCR primers used for mutants construction

Mutants	Primers[a]
M85T	TCAATGCGGGCGTC**ACG**GGCCCCCTGCCGCAAGACCTGG
	TGCGGCAGGGGGCC**CGT**GACGCCCGCATTGACGAATACC
M85S	TCAATGCGGGCGTC**AGC**GGCCCCCTGCCGCAAGACCTGG
	TGCGGCAGGGGGCC**GCT**GACGCCCGCATTGACGAATACC
M85V	TCAATGCGGGCGTC**GTC**GGCCCCCTGCCGCAAGACCTGG
	TGCGGCAGGGGGCC**GAC**GACGCCCGCATTGACGAATACC
W182V	CCATGCACCCGGGC**GTA**GTGAAAACCGACATGGGCGGCG
	ATGTCGGTTTTCAC**TAC**GCCCGGGTGCATGGCCAGCACG
L136E	TCATGAGTTCGATC**GAA**GGCAGCGTAACCATCCCCGACG
	ATGGTTACGCTGCC**TTC**GATCGAACTCATGAAGGCCAGC
L136V	TCATGAGTTCGATC**GTC**GGCAGCGTAACCATCCCCGACG
	ATGGTTACGCTGCC**GAC**GATCGAACTCATGAAGGCCAGC
M187D	GGGTGAAAACCGAC**GAC**GGCGGCGAAAACGCCGAAATCG
	GCGTTTTCGCCGCC**GTC**GTCGGTTTTCACCCAGCCCGGG
M187A	GGGTGAAAACCGAC**GCA**GGCGGCGAAAACGCCGAAATCG
	GCGTTTTCGCCGCC**TGC**GTCGGTTTTCACCCAGCCCGGG

[a]The mutated sites are underlined.

Table S2 Stereoselective reduction of halogenated acetophenones catalyzed by EbSDR8 and PpYSDR

Substrate	Stereoselectivity (ee, %)	
	EbSDR8	**PpYSDR**
1a 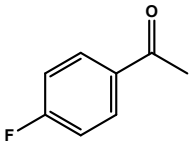	**99.7 (*R*)**	**83.2 (*S*)**
1b 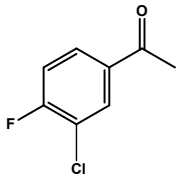	**99.9 (*R*)**	**84.5 (*S*)**
1c 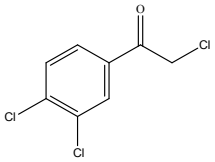	**99.3 (*S*)**	**99.5 (*R*)**
1d 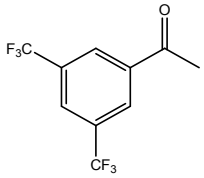	**99.8 (*R*)**	**99.9 (*S*)**
1e 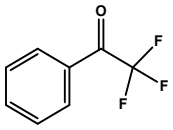	**99.4 (*S*)**	**56.8 (*R*)**
1f 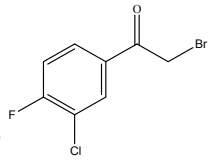	**99.0 (*S*)**	**99.6 (*R*)**

Table S3 Stereoselectivity of the wild-type PpYSDR and its single-mutation variants towards halogenated acetophenones

Substrate	WT	M85T	M85V	M85S	W182V	L136E	L136V	M187D	M187A
1a	83.2 (*S*)	30.1 (*S*)	18.2 (*S*)	46.5 (*S*)	74.6 (*S*)	77.3 (*S*)	91.6 (*S*)	79.5 (*S*)	89.0 (*S*)
1b	84.5 (*S*)	1.23 (*S*)	32.5 (*S*)	**19.0 (*R*)**	67.1 (*S*)	26.1 (*S*)	88.9 (*S*)	70.7 (*S*)	89.2 (*S*)
1c	99.5 (*R*)	53.8 (*R*)	90.4 (*R*)	65.3 (*R*)	95.5 (*R*)	95.9 (*R*)	97.7 (*R*)	85.2 (*R*)	87.3 (*R*)
1d	99.9 (*S*)	99.8 (*S*)	99.9 (*S*)	98.1 (*S*)	83.7 (*S*)	99.9 (*S*)	99.9 (*S*)	67.6 (*S*)	63.0 (*S*)
1e	56.8 (*R*)	**38.7 (*S*)**	**34.9 (*S*)**	**45.2 (*S*)**	**25.3 (*S*)**	11.5 (*R*)	**13.5 (*S*)**	25.4 (*R*)	43.9 (*R*)
1f	99.6 (*R*)	84.2 (*R*)	97.8 (*R*)	66.6 (*R*)	99.5 (*R*)	93.7 (*R*)	94.8 (*R*)	89.5 (*R*)	48.8 (*R*)

Table S4 Parameters for interactions between the protein and the substrates

Anion–π interaction (anion→aromatic ring)[a]		Distance R (Å)	Angle θ (°)	Hydrogen bond	Distance[b] (Å)	Angle (°)
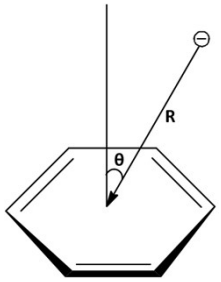	Fig S5A (4′-F atom→W182)	3.4±0.3	54.7±7.2	Fig S6B (O—H···F)	2.8±0.2	110.7±10.2
	Fig S5B (E136→Sub **1d**)	3.6±0.2	21.2±6.5	Fig 3B (O—H···Cl)	2.6±0.5	125.6±10.1
	Fig 3A (4′-F atom→W182)	3.3±0.4	64.9±8.0	Fig S7A (O—H···F)	3.1±0.3	113.4±9.6
	Fig 3B (E136→Sub **1b**)	4.0±0.2	45.9±9.2	Fig S7B (O—H···F)	3.2±0.3	126.5±9.2
	Fig 3C (D187→Sub **1d**)	4.4±0.2	64.0±7.8			

[a] Parameters for anion-π interactions: the distance (R) between the anion and the centroid of the ring; the angle (θ) between the anion-centroid vector and the principle axis of the aromatic ring[5].

[b] The distance between the oxygen atom and the halogen atom.

Table S5 Parameters of hydrogen bond between the Tyr^{150} OH and the oxygen atom of the substrate carbonyl group

Mutant-Substrate	**Tyr^{150} (O—H···O) Substrate**	
	Distance[a] (Å)	**Angle (°)**
WT-Substrate **1d** (Fig. S5A)	2.8±0.4	125.6±8.9
M85T/L136E-Substrate **1d** (Fig. S5B)	2.9±0.3	128.9±7.2
WT-Substrate **1b** (Fig. 3A)	2.9±0.3	113.6±9.1
M85T/L136E-Substrate **1b** (Fig. 3B)	3.0±0.3	125.9±5.2
M85V/M187D-Substrate **1b** (Fig. 3C)	2.9±0.4	125.4±7.8
WT-Substrate **1f** (Fig. S6A)	3.0±0.2	128.3±6.1
M85S/M187A-Substrate **1f** (Fig. S6B)	3.1±0.3	136.1±5.6
WT-Substrate **1e** (Fig. S7A)	2.7±0.3	124.5±8.2
M85V/L136V-Substrate **1e** (Fig. S7B)	3.0±0.3	135.4±9.2

[a] The distance between the oxygen atoms of Tyr^{150} OH and the substrate carbonyl group.

Table S6 Apparent kinetic parameters of PpYSDR and variants[a]

Sub[b]	Enzy[c]	K_m (mM)	K_{cat} (s^{-1})	K_{cat}/K_m (s^{-1} M^{-1})	Sub	Enzy	K_m (mM)	K_{cat} (s^{-1})	K_{cat}/K_m (s^{-1} M^{-1})
1a	WT	12.4	0.24	19	1b	WT	12.2	2.0	164
	M85T/W182V	57.8	0.77	13		M85T/W182V	8.4	1.0	119
	M85S/W182V	1011.5	15.9	16		M85S/W182V	40.3	5.4	134
	M85T/L136E	65.4	0.92	14		M85T/L136E	3.5	0.52	149
	M85V/L136V	608.5	3.8	6		M85V/L136V	8.4	0.91	108
	M85V/M187D	139.3	1.1	8		M85V/M187D	24.6	1.7	69
	M85S/M187A	555.4	5.5	10		M85S/M187A	5.8	0.67	116
1c	WT	0.24	16.5	68750	1d	WT	0.037	0.28	7568
	M85T/W182V	0.012	0.206	17167		M85T/W182V	0.063	0.28	4444
	M85S/W182V	0.033	0.39	11818		M85S/W182V	0.084	0.35	4167
	M85T/L136E	0.13	0.38	2923		M85T/L136E	0.051	0.36	7059
	M85V/L136V	0.49	0.84	1714		M85V/L136V	0.051	0.033	6471
	M85V/M187D	0.015	0.29	19333		M85V/M187D	0.63	1.34	2127
	M85S/M187A	0.022	0.29	13182		M85S/M187A	0.046	0.30	6522
1e	WT	3.4	4.0	1177	1f	WT	0.21	1.1	5238
	M85T/W182V	154.2	37.1	241		M85T/W182V	0.11	0.31	2818
	M85S/W182V	30.6	7.6	248		M85S/W182V	0.21	0.35	1667
	M85T/L136E	4.0	1.1	275		M85T/L136E	0.21	0.29	1381
	M85V/L136V	4.5	3.4	756		M85V/L136V	0.16	0.36	2250
	M85V/M187D	9.8	3.2	327		M85V/M187D	0.27	0.36	1333
	M85S/M187A	14.5	5.1	352		M85S/M187A	0.12	0.31	2583

[a] Experiments were performed in triplicate and mean values are presented;

[b] Abbreviation for substrate;

[c] Abbreviation for enzyme.

Supplementary Figures

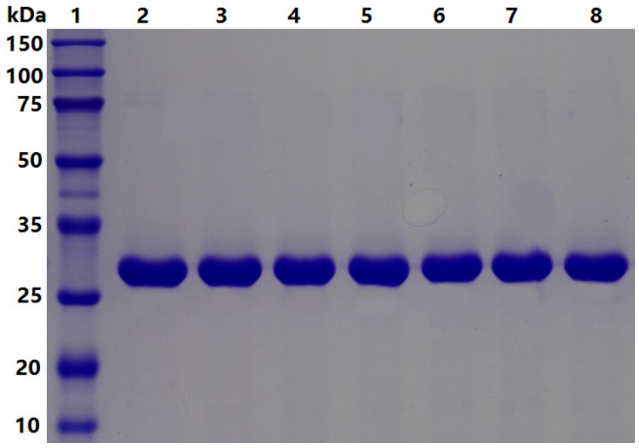

Fig. S1 SDS-PAGE (12%) analysis of the purified PpYSDR and its mutations. Lane 1, molecular weight marker; lane 2, wide-type PpYSDR ; lane 3, M85T/W182V; lane 4, M85S/W182V; lane 5, M85T/L136E; lane 6, M85V/L136V; lane 7, M85V/M187D; lane 8, M85S/M187A.

The gene *Ppysdr* was obtained from the genomic DNA of *P. putida* ATCC 12633 by PCR amplification using the primers (PpYSDRF/PpYSDRR) designed according to the SDR sequence of annotated genome from *P. putida* NBRC 14164 (Genbank accession number AP013070). The full-length sequence of *Ppysdr* was 687 bp, encoding a 228 amino acids polypeptide with a calculated molecular mass of 24.5 kDa and a putative isoelectric point of 5.07 (http://web.expasy.org/protparam/). The *Ppysdr* gene was subsequently overexpressed in *E. coli* BL21(DE3) using the pET30a expression vector. The recombinant PpYSDR with an N-terminal His-tag was purified to electrophoretic homogeneity by nickel affinity chromatography. The purified enzyme migrated as a single band with a molecular weight of approximately 30.0 kDa on SDS-PAGE (Fig. S1), consistent with the theoretical molecular mass of the His-tagged protein.

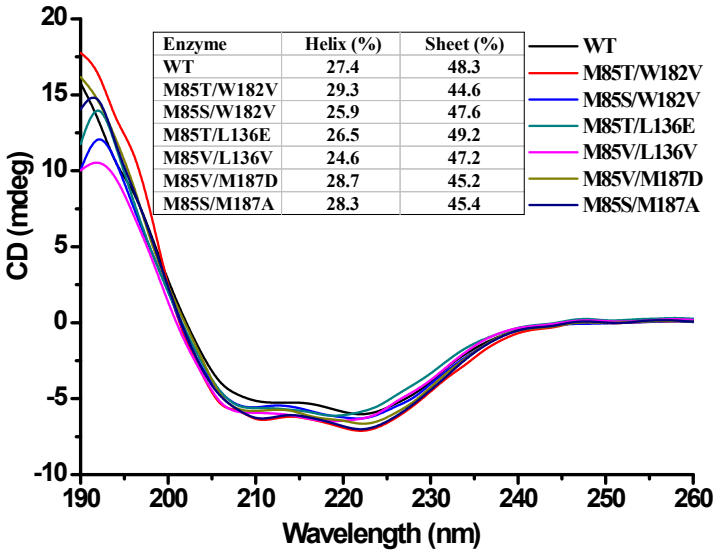

Fig. S2 CD spectra for the wild-type PpYSDR and variants.

The percentage of α-helix and β-sheet structure was measured as an indication of correct folding of the protein by circular dichroism (CD) spectroscopy. The CD spectra for the wild-type PpYSDR and variants were recorded between 190 and 260 nm (Fig. S2), and the secondary structure content was estimated. As shown in Fig. S2, there was no pronounced difference in the α-helix and β-sheet content between the wild-type PpYSDR and variants.

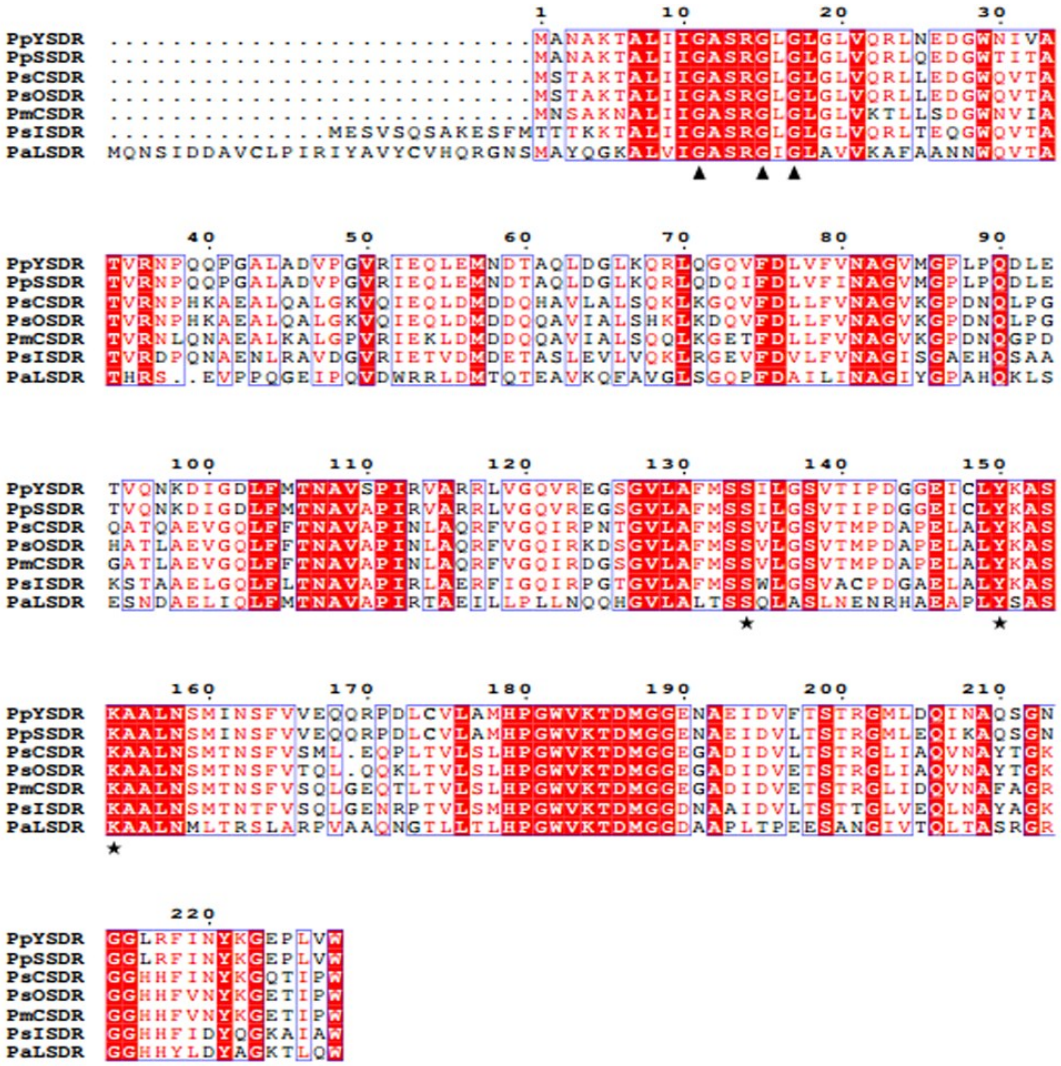

Fig. S3 Multi-alignment of amino acid sequences between PpYSDR and its close homologues. PpSSDR from *P. putida* S11 (96% identity; EJT85574); PsCSDR from *Pseudomonas* sp. CMAA1215 (63% identity; ERO62642); PsOSDR from *Pseudomonas* sp. Os17 (63% identity; BAQ72411); PmCSDR from *P. mediterranea* CFBP 5447 (62% identity; KGU87299); PsISDR from *P. syringae* pv. actinidiae ICMP 19096 (61% identity; EPN35816); PaLSDR from *Pantoea ananatis* LMG 20103. The sequence alignment revealed that the enzyme shared the highly conserved amino acid residues with all other typical SDRs. For example, the coenzyme NAD(P)H binding motif $G^{11}XXXG^{15}XG^{17}$ was conserved in the N-terminal region of PpYSDR, which is the glycine-rich "fingerprints" sequence of the SDR superfamily[6], as well as the conserved catalytic triad (Ser^{134}-Tyr^{150}-Lys^{154}). The sequence alignment is visualized using ESPript 2.2. The numbering shown is according to the sequence of PpYSDR. Triangles, critical coenzyme binding residues; stars, putative conserved catalytic residues (S134, Y150, and K154). Strictly conserved residues are highlighted with red boxes.

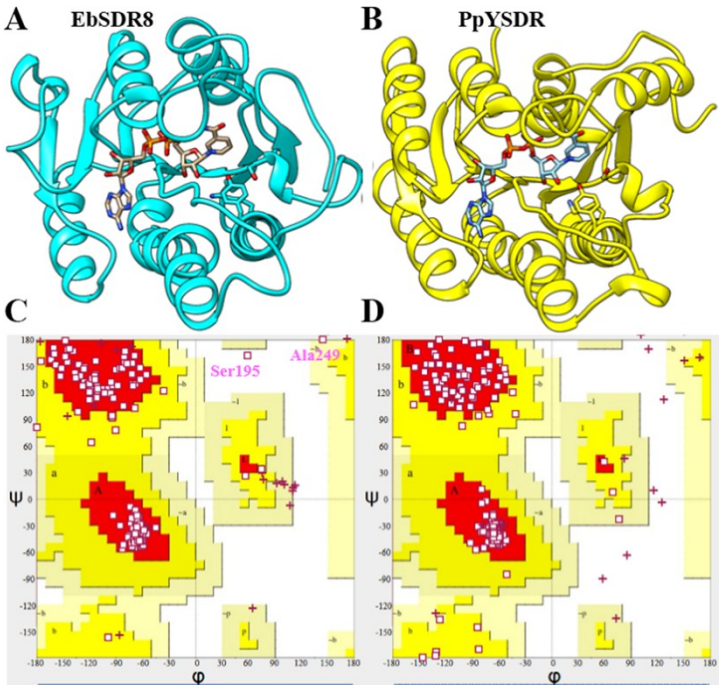
A
EbSDR8
B
PpYSDR
C
D
Ser195
Ala249
Ψ
Φ

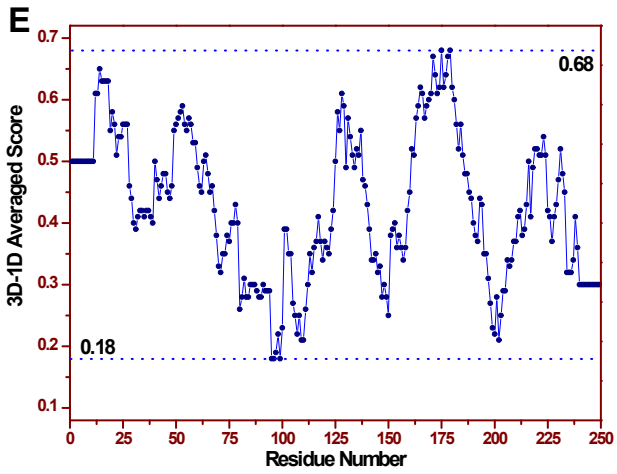
E
3D-1D Averaged Score
0.68
0.18
Residue Number

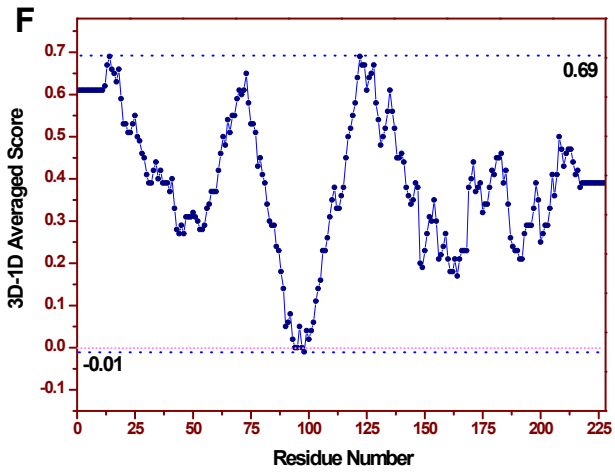
F
3D-1D Averaged Score
0.69
-0.01
Residue Number

Ramachandran plot statistics	EbSDR8		PpYSDR	
Residues in most favoured regions [A,B,L]	198	94.3%	175	92.1%
Residues in additional allowed regions [a,b,l,p]	10	4.8%	13	6.8%
Residues in generously allowed regions [~a,~b,~l,~p]	1	0.5%	2	1.1%
Residues in disallowed regions [XX]	1	0.5%	0	0.0%
Number of non-glycine and non-proline residues	210	100%	190	100%
Number of end-residues (excl. Gly and Pro)	3		3	
Number of glycine residues	30		26	
Number of proline residues	8		10	
Total number of residues	251		229	

Fig. S4 Procheck-Ramachandran plots and 3D-profile window plots of the Verify 3D server for the homology models of PpYSDR and EbSDR8 obtained by homology modelling and the corresponding Ramachandran plot statistics. A and B: 3D structural models of EbSDR8 (A) and PpYSDR (B); C and D: Ramachandran plots for structural models of EbSDR8 (C) and PpYSDR (D); E and F: 3D-profile window plots for the homology models of EbSDR8 (E) and PpYSDR (F).

The Ramachandran plot distribution indicated that both structures had over 92% of residues in the most favored orientation. The model of PpYSDR had no residues in disallowed region. In the case of EbSDR8, the only residue (Ser^{195}) in disallowed region was later shown to be away from the catalytic cavity. Therefore, we could conclude that the structural models agreed well with the expected conformational space for residues. In addition, the 3D-1D averaged profile analysis of the Verify 3D server showed a reliable folding in most regions of both models (PpYSDR: 90.35% of the residues had an averaged 3D-1D score >= 0.2; EbSDR8: 98.40% of the residues had an averaged 3D-1D score >= 0.2). In summary, the overall assessment indicated that both models had a satisfactory accuracy for further structure-based analysis.

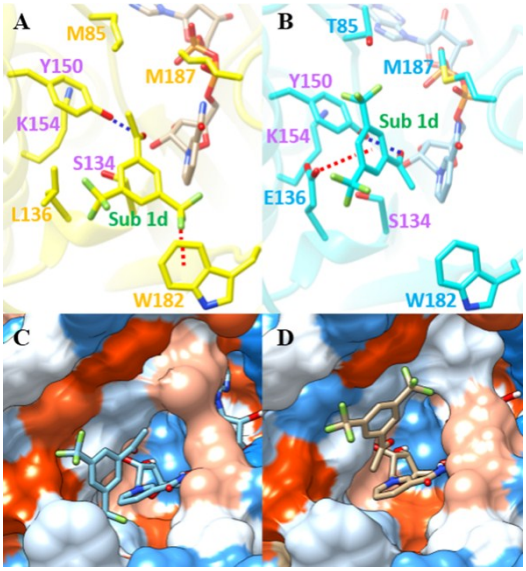

Fig. S5 Comparison of preferred conformations of substrate **1d** docked in the active sites of enzymes. Figure S5A and S5C are figure of substrate **1d** binding to the wild type. Figure S5B and S5D are figure of substrate **1d** binding to mutant M85T/L136E. Red dash lines, the interactions involving the aromatic ring (parameters shown in Table S4); Blue dash lines, hydrogen bonds involving Tyr150 OH and oxygen atom of the substrate carbonyl group (parameters shown in Table S5).

In the docking studies of substrate **1d** into the mutant M85T/L136E, the anion-π interaction between the carboxylic moiety of glutamate and the aromatic ring of the substrates was involved (Fig. S5B).

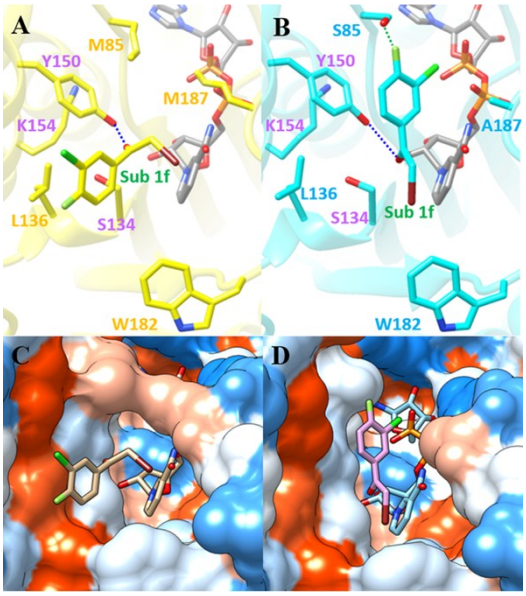

Fig. S6 Comparison of preferred conformations of substrate **1f** docked in the active sites of enzymes. Figure S6A and S6C depict substrate **1f** bound to the wild type. Figure S6B and S6D show substrate **1f** bound to mutant M85S/M187A. Green dash line, hydrogen bond involving the halogen atom of the substrate (parameters shown in Table S4); Blue dash lines, hydrogen bonds involving Tyr^{150} OH and oxygen atom of the substrate carbonyl group (parameters shown in Table S5).

In the case of M85S/M187A, the only mutant exhibiting reversed stereoselectivity towards substrate **1f**, the active cavity was dramatically expanded relative to the wide-type PpYSDR (Fig. S6).

It was clearly demonstrated by docking results that the decreased steric hindrance adequately enlarged the small pocket to accommodate the large group of aryl substrates and thus facilitated the binding of substrates with an anti-Prelog preferred conformation (Fig. 3B, 3C, S5C, S5D, S6C and S6D). On the other hand, due to the limited space, a larger substrate will be less likely to have alternative binding modes, which may result in relatively stable stereoselectivity. The single-mutation variants of M85 provide the most striking evidence for the above assumption. The substitutions of M85 exerted only marginal effect on the stereoselectivity towards the largest substrate **1d**, while the same variants showed significantly decreased or even reversed stereoselectivity toward other relatively smaller substrates (Table S3).

The fluorine atom of substrate **1f** formed hydrogen bond with the serine OH group of M85S/M187A (Fig. S6B).

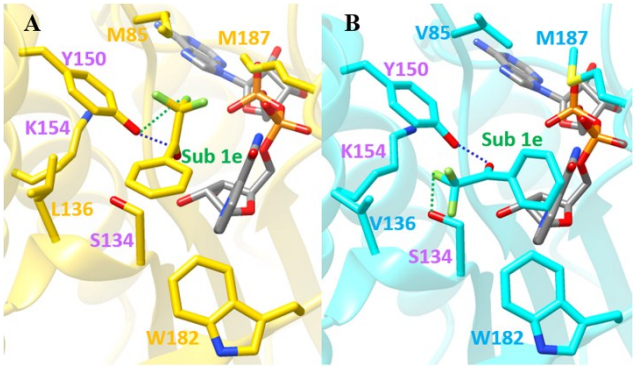

Fig. S7 Comparison of preferred conformations of substrate **1e** docked in the active sites of enzymes. Figure S7A depict substrate **1e** bound to the wild type. Figure S7B show substrate **1e** bound to mutant M85V/L136V. Green dash lines, hydrogen bonds involving halogen atom of substrate (parameters shown in Table S4); Blue dash lines, hydrogen bonds involving Tyr^{150} OH and oxygen atom of the substrate carbonyl group (parameters shown in Table S5).

Substrate 1a Retention time: substrate, 4.7 min; *R*-product, 6.9 min; *S*-product, 7.1 min.

WT

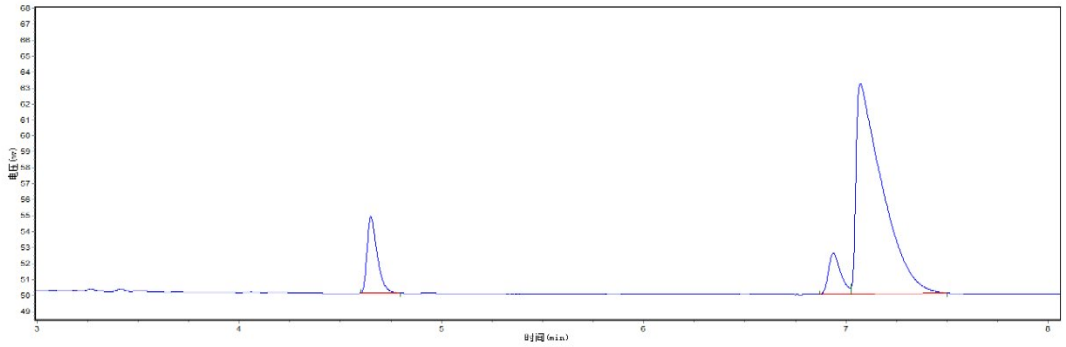

M85T/W182V

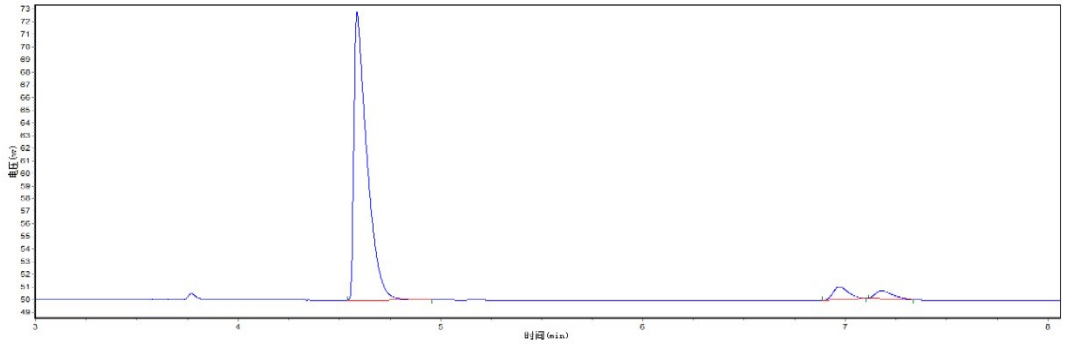

Substrate 1b Retention time: substrate, 5.3 min; *R*-product, 9.4 min; *S*-product, 9.7 min.

WT

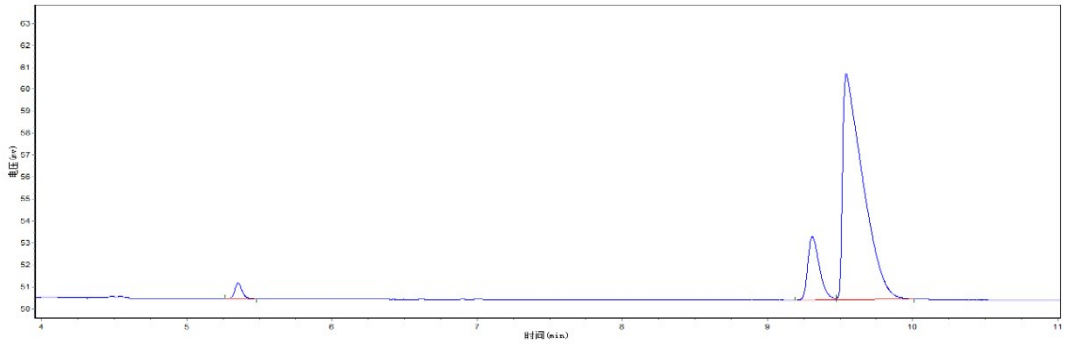

M85V/M187D

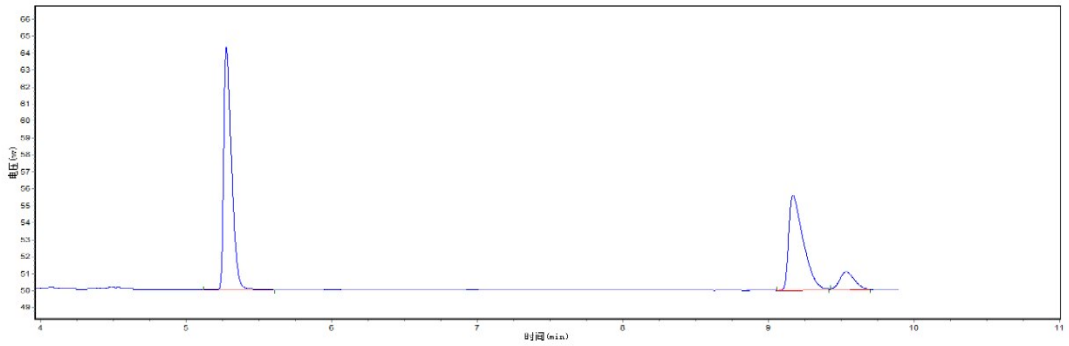

Substrate 1c Retention time: substrate, 7.6 min; *R*-product, 10.6 min; *S*-product, 11.0 min.

WT

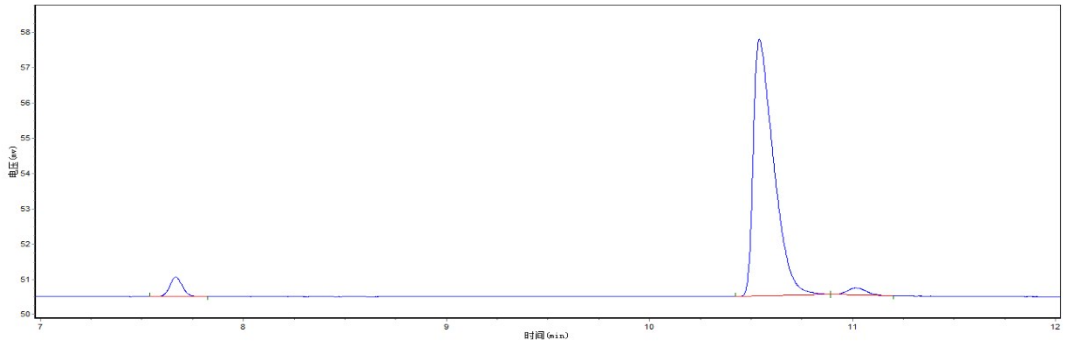

M85S/W182V

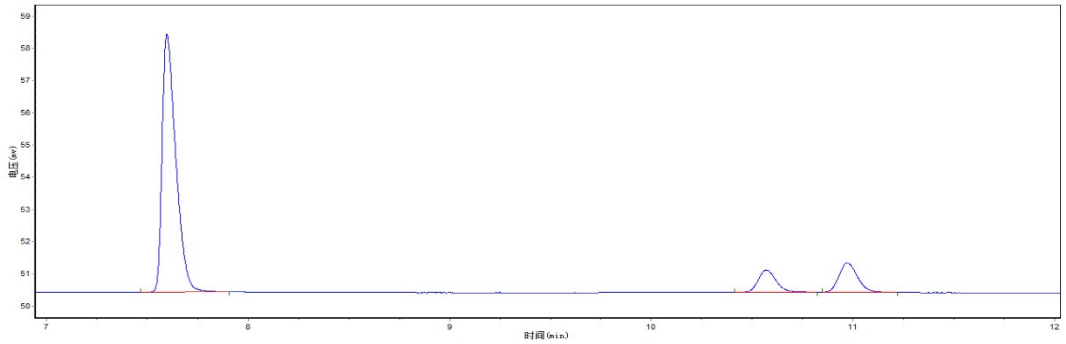

Substrate 1d Retention time: substrate, 4.8 min; *S*-product, 12.0 min; *R*-product, 12.4 min.

WT

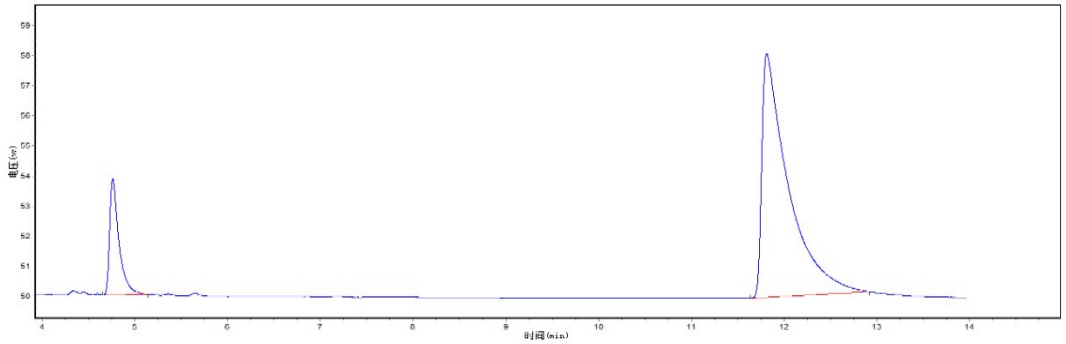

M85T/L136E

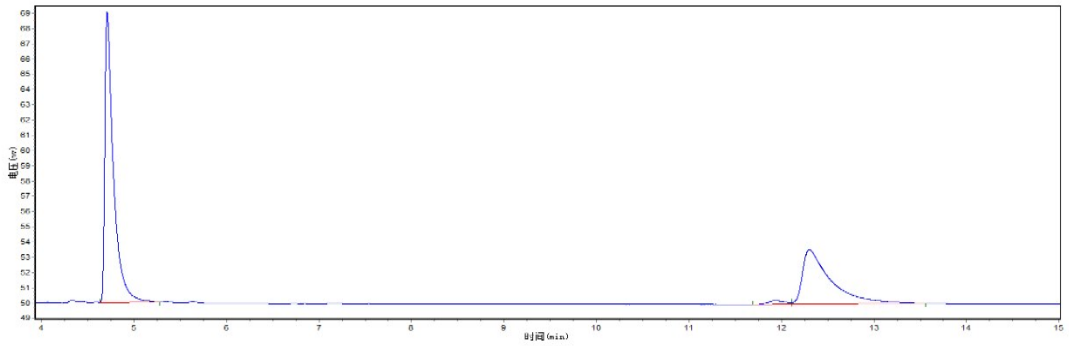

Substrate 1e Retention time: substrate, 1.9 min; *S*-product, 5.6 min; *R*-product, 5.9 min.

WT

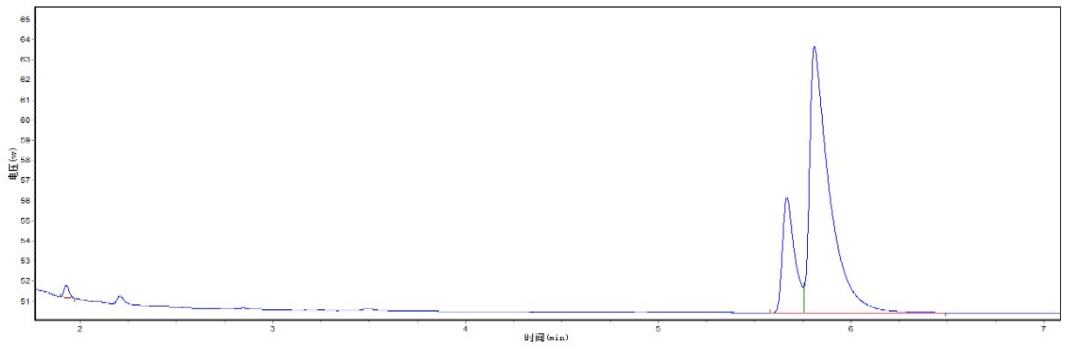

M85T/W182V

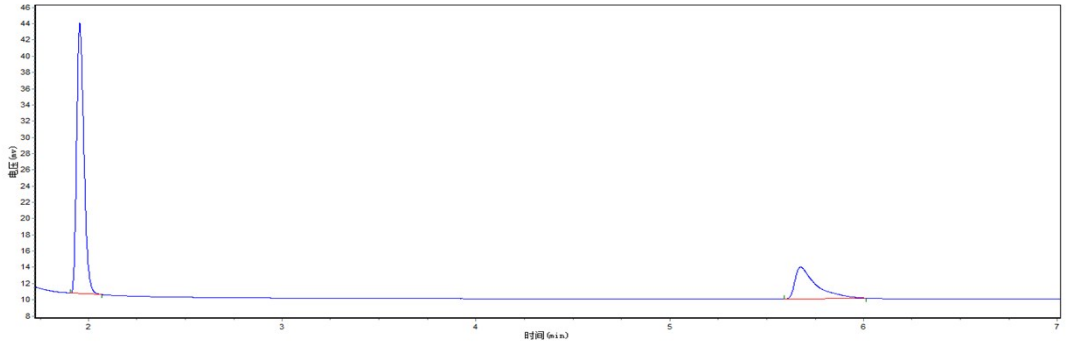

Substrate 1f Retention time: substrate, 5.1 min; *R*-product, 7.8 min; *S*-product, 8.0 min.

WT

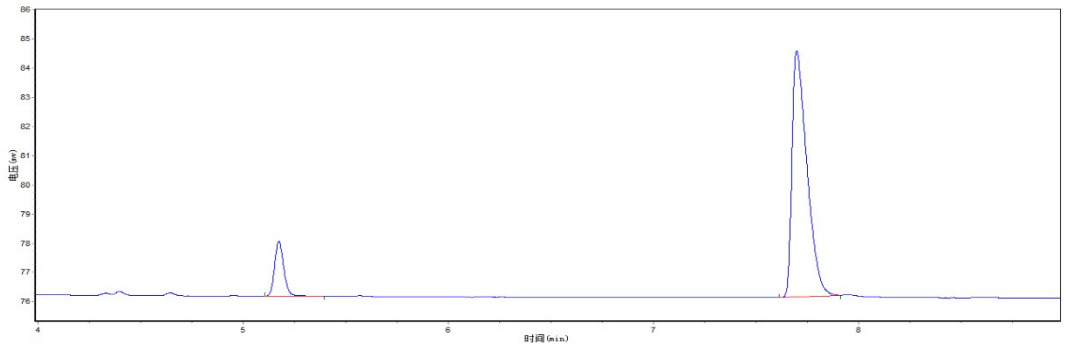

M85S/M187A

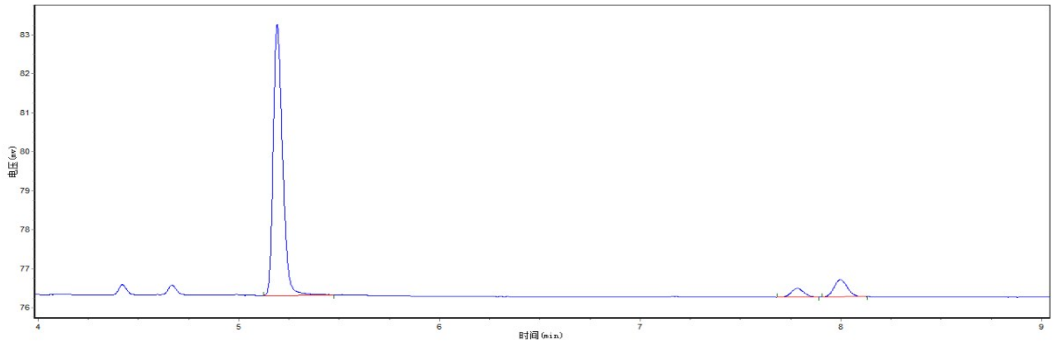

Fig. S8 The chiral GC chromatograms of the reduction products of halogenated acetophenones by the wild-type PpYSDR and selected mutants.

Reference

1. M. M. Bradford, *Anal Chem*, 1976, **72**, 248-254.
2. A. Li, L. Ye, H. Wu, X. Yang and H. Yu, *Journal of Molecular Catalysis B: Enzymatic*, 2015, **122**, 179-187.
3. J. Gu and H. Yu, *Journal of Biomolecular Structure and Dynamics*, 2012, **30**, 585-593.
4. O. Trott and A. J. Olson, *Journal of computational chemistry*, 2010, **31**, 455-461.
5. M. V. Z. ic, S. Z. Borozan, M. R. Nikolic´ and S. Đ. Stojanovic, *RSC Advances*, 2015, **5**, 38361-38372.
6. Z. Wang, Q. Song, M. Yu, Y. Wang, B. Xiong, Y. Zhang, J. Zheng and X. Ying, *Appl Microbiol Biotechnol*, 2014, **98**, 641-650.